Preparation and Characterization of Magnetic Carbon Nanospheres for the Demulsification of Water-in-Oil Emulsion

Shijun Guo, Lixin Wei,* and Lin Zhang

ACCESS | 📊 Metrics & More | 📖 Article Recommendations

ABSTRACT: In order to reduce the harmful effects of demulsifiers on the environment and provide a green and reusable demulsifier, a magnetic carbon nanosphere demulsifier (Fe_3O_4/CNNs) was prepared in this study. The morphology and structure of the Fe_3O_4/CNNs were characterized by scanning electron microscopy, Fourier transform infrared, X-ray diffraction, and X-ray photoelectron spectroscopy. The results showed that the magnetic demulsifier has uniform particles and good dispersibility. In addition, the demulsification experiments showed that the dehydration rate could reach 92% under the optimal demulsification conditions, and the residual water content of Fe_3O_4/CNN magnetic demulsifier increased by 0.11% in 8 cycles of recovery experiments. The demulsification mechanism of the demulsifier was speculated. This work showed that the compounded magnetic demulsifier is friendly to the environment and is an effective material for separating oil and water phases, with broad application prospects.
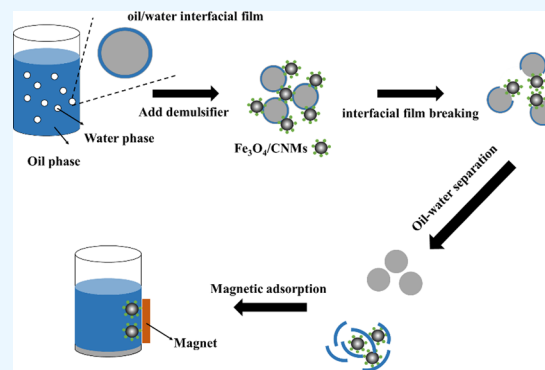
1. INTRODUCTION

At present, the problem of crude oil demulsification has gradually become one of the problems plaguing researchers. When crude oil was extracted from the formation, oil was mixed with groundwater, resulting in a high water content of the produced fluid.[1] The existence of the emulsion led to problems such as pipeline scaling and corrosion, so it is necessary to separate the oil and water phases.[2] Traditional demulsifiers such as phenolic resin polyether and phenolic resin polyether are widely used in demulsification.[3] Different from the physical demulsification methods, the chemical demulsification methods do not require huge equipment, high capital, and high maintenance costs.[4] At present, the research on traditional demulsifiers are mainly divided into the following categories, including ethylene oxide and propylene oxide block polyethers,[5] hyperbranched poly(amido amine) demulsifiers,[6] cellulose derivative polymers,[7] and ionic liquids.[8] However, one disadvantage of these demulsifiers is that they are not reusable.

Therefore, magnetic demulsifiers have developed rapidly in recent years.[9] Currently, Fe_3O_4 magnetic nanoparticles have become a hot research topic due to their excellent properties such as relatively low cost and good compatibility. The grafting of other materials or surfactants on the surface of Fe_3O_4 magnetic nanoparticles improved the dispersibility of Fe_3O_4 and also increased the demulsification efficiency. The method of synthesizing magnetic demulsifiers is to first synthesize Fe_3O_4 magnetic nanoparticles, and then compound them with other particles. Lü et al.[10] synthesized a series of quaternized chitosan (QC)-grafted magnetic nanoparticles (MNPs) successfully

synthesized for demulsification from aqueous environments. First, Fe_3O_4 was synthesized by the co-precipitation method followed by surface coating with silica and aminopropyl to form a surface for further grafting of QC molecular chains. Their demulsification performances were evaluated in detail as a function of dosage, QC grafting ratio (Gq), pH, and magnetic field. The results showed that pH did not significantly affect the oil−water separation performance and MNPs with high Gq exhibited enhanced separation efficiency. The separation capacity was estimated to be >105 mg of diesel oil/mg of magnetic flocculant. The recycling experiment indicated the magnetic flocculant could be recycled up to at least 7 cycles at various pH levels. However, this method of synthesizing magnetic demulsifiers is complicated. Therefore, there are also many studies that add other particles to synthesize composite materials while synthesizing Fe_3O_4 MNPs. Zhao et al.[11] successfully synthesized polyethyleneimine (PEI)-coated Fe_3O_4 magnetic nanoparticles by a one-step solvothermal method. The synthesized demulsifiers were characterized. An oil-in-water emulsion was prepared and the demulsification ability of the prepared magnetic demulsifier was evaluated. The
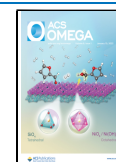
results show that the demulsifier was successfully adsorbed at the O/W interface of the emulsion. As a result, the oil−water interface was rapidly destabilized and coalesced under the applied magnetic field. The results of the demulsification experiments showed that the PEI-coated Fe_3O_4 could be reused up to ten times in recovery experiments at different pH levels. This showed the good ability to reuse.

At present, many studies combine Fe_3O_4 with chemical demulsifiers that have been widely used in oil fields. Li et al.[12] prepared $Fe_3O_4@SiO_2$ followed by $Fe_3O_4@SiO_2$-epoxy resin using (3-glycidoxypropyl) trimethoxysilane as a silane coupling agent. Then, a demulsifier called 5010 was used to react with the epoxy groups on the surface of $Fe_3O_4@SiO_2$-epoxy resin to prepare M-5010 demulsifier. Demulsification experiments were performed on two demulsifiers. Under the same conditions, the demulsification rate of M-5010 was higher than that of 5010. Although these magnetic demulsifiers have excellent performance, the chemical demulsifiers contained in the magnetic demulsifiers will affect the environment, and the preparation process is relatively complex. Therefore, it is extremely important to develop a green and environmentally friendly magnetic demulsifier. Carbon nanomaterials have become a hot topic of research due to their special properties and have been widely studied and applied in capacitors,[13] catalysis,[14] medical science[15] and other fields. Huang[16] synthesized a magnetic recyclable carbon nanotube demulsifier ($CNTs/Fe_3O_4$), and the demulsification efficiency in oily wastewater reached 99.6% under optimal conditions and the total organic carbon of the separated water was reduced to 32.8 mg/L. Moreover, the recyclability test indicated that $CNTs/Fe_3O_4$ could be reused four times without significant reduction in light transmittance. Carbon nanospheres (CNNs) are one of the CNN materials.[17] Compared with other material nanomaterials, CNNs can provide greater pore accessibility and faster molecular diffusion/transfer, and due to the $\pi-\pi$ conjugated system contained in the carbon nanomaterials,[18] it is presumed that it will have a good effect on emulsion demulsification.

Therefore, in this study, a magnetic CNNs demulsifier ($Fe_3O_4/CNNs$)) was synthesized by adding CNNs directly to the synthesis of Fe_3O_4 in a "one-step" process. Due to the abundant hydrophilic oxygen-containing groups on the surface of CNNs and the lipophilic of oleic acid, $Fe_3O_4/CNNs$ are amphiphilic and can quickly destroy the oil−water interfacial film. This work provides an alternative method to separate the oil and water phases and can also provide some inspiration for the future development of magnetic demulsifiers.

2. EXPERIMENTAL SECTION

2.1. Materials.
CNTs, oleylamine, and dibenzyl ether were purchased from Shanghai Macklin Biochemical Co., Ltd.; glucose and n-hexane were purchased from Tianjin Kaitong Chemical Reagent Co., Ltd.; anhydrous ethanol and oleic acid were purchased from Tianjin Tianli Chemical Reagent Co., Ltd.; iron acetylacetonate was purchased from Shanghai Rhawn Chemical Technology Co., Ltd.; octadecene was purchased from Sinopharm Chemical Reagent Co., Ltd. Specifications for above materials are AR.

2.2. Preparation of CNNs.[19]
First, 10 g of glucose and 100 mL of deionized water were mixed well. Then the glucose solution was poured into a reaction kettle. The solution was heated at 180 °C for 12 h. After the reaction, a brown-black solution was obtained. After the reaction, a brown-black solution was obtained, which was washed three times with deionized

water and anhydrous ethanol and dried at 60 °C. The final brown-black CNNs were obtained. The reaction mechanism is that glucose can undergo aromatization through dehydration and decomposition between isomerization molecules under hydrothermal conditions to generate aromatic compounds. In this process, C=O and C=C bonds can be realized through dehydration within the monomer and structural alternation of enols or intramolecular dehydration. Aromatic compounds and other macromolecular polymer molecules in the solution will continue deep dehydration polymerization to form aromatic clusters with a higher polymerization degree. When the dosage of these highly polymerized macromolecules reaches a certain saturation critical dosage, a carbon nucleus will be formed. Through diffusion, organic molecules and macromolecules in the solution will deposit and shrink on the surface of carbon nucleus to form carbon spheres.

2.3. Preparation of Magnetic Fe_3O_4/CNN Demulsifier.
$Fe_3O_4/CNNs$ were prepared a by one-pot method). First, a certain quantity of iron acetylacetonate, oleylamine, oleic acid, and octadecene was mixed well and a certain quantity of CNNs was added. Subsequently, all materials were mixed well by ultrasonic dispersion in the solvent dibenzyl ether. The mixture was poured into a polyparaphenol material liner, put into a reaction kettle, and reacted at 230 °C for 5 h. After the reaction, the product was adsorbed with a magnet and washed repeatedly with a mixture of anhydrous ethanol and hexane at a volume ratio of 1:1. The product was dried at 65 °C for 12 h to obtain $Fe_3O_4/CNNs$. The specific schematic of Fe_3O_4 is shown in Figure 1.
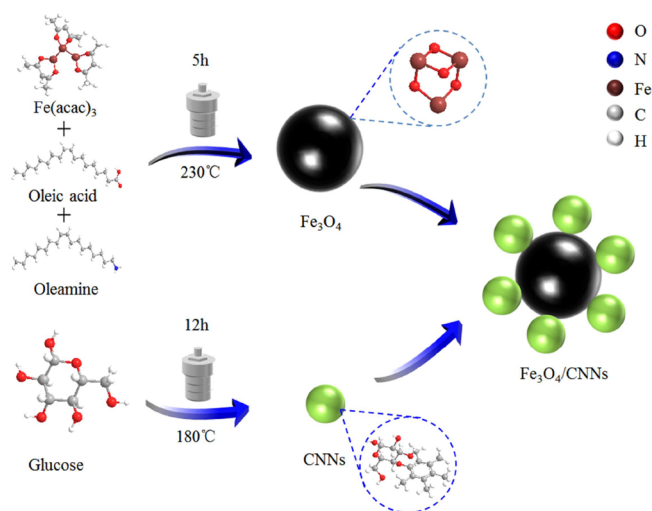
Figure 1. Synthesis schematic of Fe_3O_4, CNNs, and $Fe_3O_4/CNNs$.

2.4. Demulsification Test.
First, simulated emulsion was prepared. 500 mL of toluene and 5 mL of deionized water were added to a round-bottomed flask, and 1 g of span80 was added to the mixture. The electric stirrer was started and the water-in-toluene emulsion was prepared by stirring continuously for 5 h at a rotation speed of 3000 rpm/min. The demulsification performance of the magnetic carbon nanomaterial demulsifier was evaluated by using the bottle test method. First, the emulsion was added to a glass bottle. Then a certain dosage of demulsifier was added to the emulsion and the glass bottle was shaken 100 times in 30s to make the demulsifier completely dispersed in the emulsion. The demulsification effect was observed after 5 min. After the demulsification experiment, the
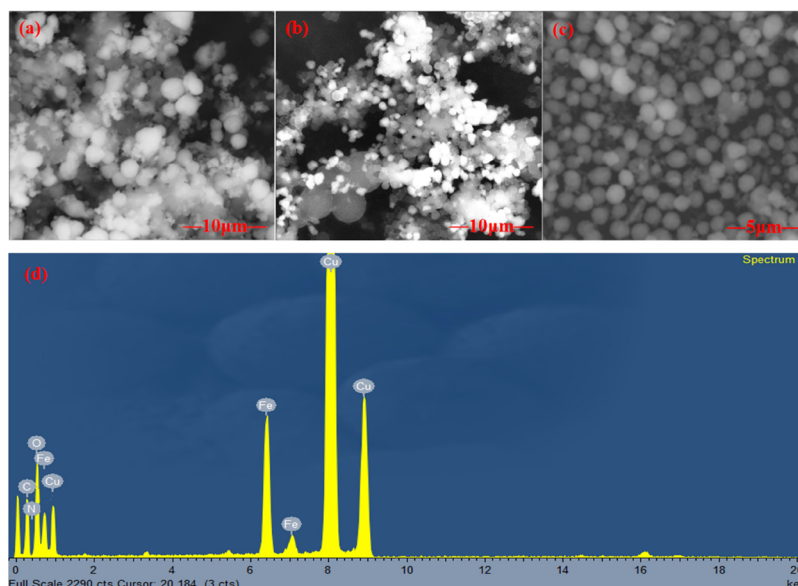
Figure 2. Scanning electron microscopy (SEM) images of CNNs and Fe$_3$O$_4$/CNNs (a: CNNs; b: Fe$_3$O$_4$/CNNs; c: Fe$_3$O$_4$; d: energy dispersive spectroscopy (EDS) mapping of Fe$_3$O$_4$/CNNs).

residual water content in the oil phase was determined using Karl Fischer moisture determination instrument, and the data were recorded.

## 3. RESULTS AND DISCUSSION

3.1. Scanning Electron Microscopy of Fe$_3$O$_4$/CNNs. Figure 2a shows that the CNNs have a spherical shape, uniform particle size, and good dispersion. Figure 2b,c shows the morphology of Fe$_3$O$_4$ and it can be observed that there are well-dispersed small spheres, and indistinct larger spherical structures. This is because the conductivity of Fe$_3$O$_4$ is stronger than that of CNNs. It can be seen from Figure 2c that Fe$_3$O$_4$ is relatively uniformly distributed, and no obvious agglomeration is observed. Figure 2d is the EDS mapping of Fe$_3$O$_4$/CNNs. In addition to the presence of Fe, Cu, O, and other elements, the presence of C element can also be detected in the Fe$_3$O$_4$/CNNs, which proves that the CNNs are successfully compounded with Fe$_3$O$_4$.

3.2. Fourier Transform Infrared Spectroscopy of Fe$_3$O$_4$/CNNs. Figure 3 shows the FTIR spectra of CNNs, Fe$_3$O$_4$, and Fe$_3$O$_4$/CNNs. It can be seen in Figure 3 that the peak at 3380.81 cm^{-1} is ascribed to −OH. The −OH in CNNs is produced during the hydrolysis of glucose. The −OH in Fe$_3$O$_4$ and Fe$_3$O$_4$/CNNs is from the oleic acid that were not removed cleanly. Meanwhile, the presence of C=C in CNNs is demonstrated from the peak at 1709.42 cm^{-1}. In addition, the FT-IR spectra of CNNs show the presence of C=O at the peak of 1611.48 cm^{-1}. These peaks can also be found in Fe$_3$O$_4$/CNNs, which proves the presence of CNNs in the Fe$_3$O$_4$/CNNs. The peak at 554.41 cm^{-1} indicates the Fe−O, and it can be found in the FT-IR spectra of both Fe$_3$O$_4$ and Fe$_3$O$_4$/CNNs, proving that Fe$_3$O$_4$ has been successfully compounded with CNNs. In addition, comparing the FT-IR spectra of CNNs and Fe$_3$O$_4$/CNNs, the intensities of all peaks were significantly weakened in Fe$_3$O$_4$/CNNs. This is due to the CNNs being occluded by Fe$_3$O$_4$, which leads to the weakening of the peak intensity of the composites.

**3.3. X-ray Diffraction of Fe$_3$O$_4$/CNNs.** In order to further verify the successful synthesis of Fe$_3$O$_4$/CNNs and the phase
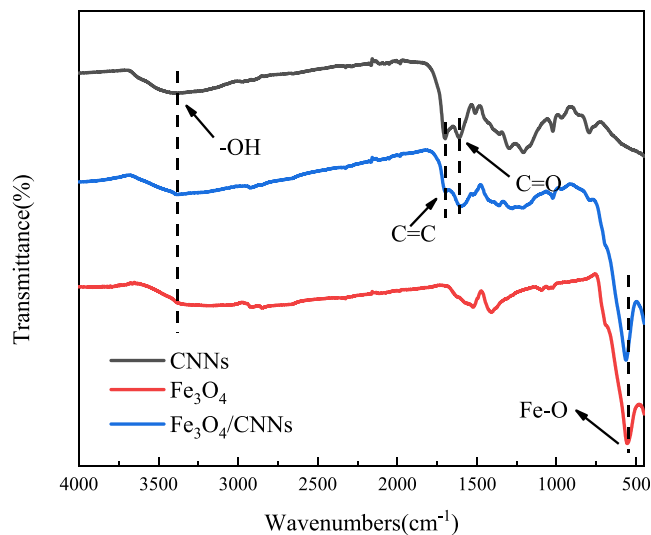
Figure 3. Fourier transform infrared spectroscopy (FTIR) spectra of CNNs, Fe$_3$O$_4$, and Fe$_3$O$_4$/CNNs.

change in the reaction process, the synthesized product was characterized by XRD. The diffraction peaks of the three substances in Figure 4 are very distinct. In the peaks at 2θ = 20.87°, one prominent peak appears in the XRD pattern of the CNNs. The width of this peak indicates the low crystallinity of CNNs. Also six diffraction peaks appeared in the XRD pattern for Fe$_3$O$_4$/CNNs. The peaks at 2θ = 30.17° (220), 35.47° (311), 43.17° (400), 53.43° (422), 57.17° (511), and 62.63° (440) are consistent with the XRD standard card of Fe$_3$O$_4$ (JCPDS Card No. 19-0629).[20] In addition, it can be seen from the XRD pattern that the diffraction peak intensity of Fe$_3$O$_4$/CNNs at 20.87° is low, which can be attributed to two points: 1. The crystallinity of Fe$_3$O$_4$ is higher than that of CNNs, which leads to a lower intensity of CNN diffraction peaks; 2. Less mass of CNNs was added during the preparation process, which resulted in lower intensity of diffraction peaks.
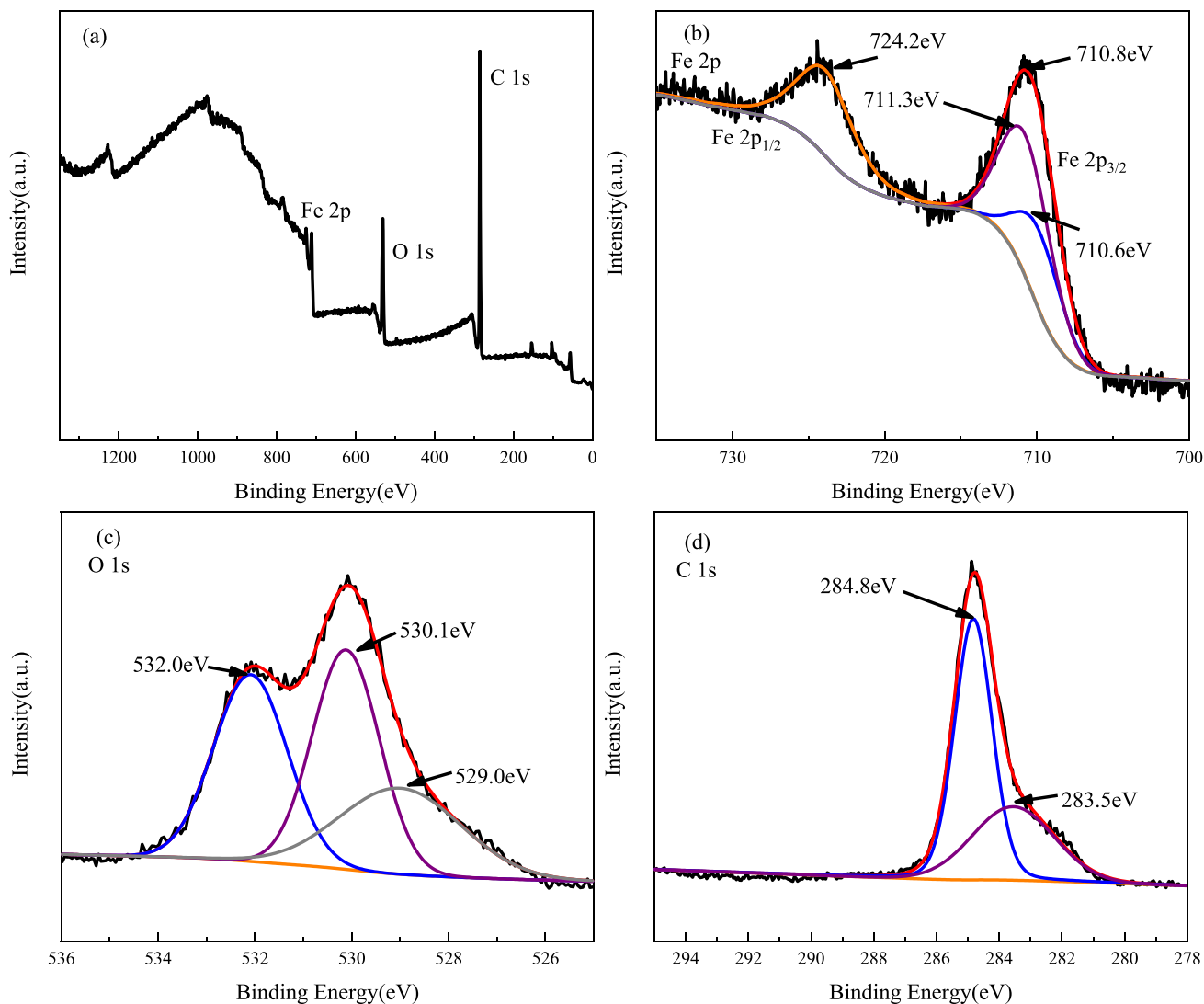
3.4. X-ray Photoelectron Spectroscopy of Fe$_3$O$_4$/CNNs. From Figure 5a, it can be seen that there are Fe, O, and C
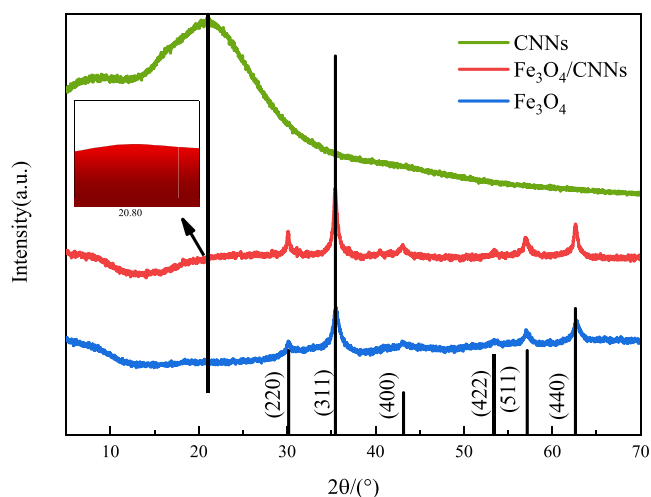
**Figure 4.** X-ray diffraction (XRD) pattern for CNNs, Fe_3O_4/CNNs, and Fe_3O_4.

elements in the Fe_3O_4/CNNs. From the Fe 2p pattern in Figure 5b, it can be seen that the characteristic peaks for Fe2p1/2 at 724.2 eV and Fe2p3/2 at 710.8 eV are exhibited, while no satellite peaks (718.8 and 729.5 eV) are found near the characteristic peaks, this is characteristic of Fe_3O_4. In addition, the characteristic peaks at Fe2p3/2 were deconvoluted to obtain two peaks at 710.6 and 711.3 eV, which correspond to Fe^{2+} and Fe^{3+}, respectively. The peak areas of the two peaks were calculated to be 0.35:0.69, which is obviously within the error range compared with the theoretical value and proves the successful synthesis of Fe_3O_4.[20]

In addition, there is a 530.1 eV characteristic peak in the O 1s pattern of Figure 5c, and the peak represents the characteristic peak of lattice oxygen in Fe_3O_4. The characteristic peak at 532.0 eV is the oxygen of the carboxylate complexed on Fe. Theoretically, there should be two characteristic peaks formed by mono and bidentate carboxylates, however, the measurement resolution is not sufficient, so only the characteristic peak of the monodentate complex is shown.[21] The C 1s pattern in Figure 5d at 284.8 eV is the characteristic peak of C in oleic acid and CNNs and the weak characteristic peak at 283.5 eV appeared during the

Figure 5. X-ray photoelectron spectroscopy (XPS) pattern for the synthesized products (a: Whole pattern of Fe_3O_4/CNNs; b: Fe 2p pattern of Fe_3O_4/CNNs; c: O 1s pattern of Fe_3O_4/CNNs; d: C 1s pattern of Fe_3O_4/CNNs).
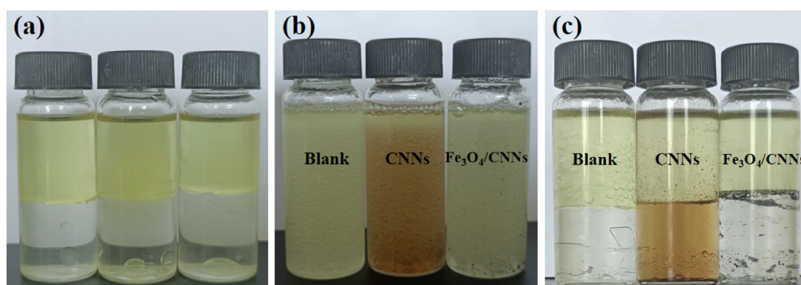
Figure 6. Interfacial activity of different materials (a: diesel/water interface; b: after shaking for 200 times; c: after settling for 20 min).

peak separation may be a byproduct generated during the preparation process.[22]

3.5. Interfacial Activity of Fe₃O₄/CNNs. The interfacial activity was studied by observing the distribution of different materials at the oil−water interface. First, 10 mL diesel and 10 mL distilled water were added into the test tube, the oil−water interface was clear, as shown in Figure 6a. Then 0.01 g CNNs and Fe₃O₄/CNNs were added to the other two test tubes, respectively, and the tubes was sharply shaken 200 times. Figure 6b shows that the oil−water interface disappeared in the control group, while CNN and Fe₃O₄/CNN solutions became turbid. It can be seen from Figure 6c that after standing for 20 min, the oil−water separation phenomenon was obvious in the control group. CNNs were almost all distributed in the water phase, because CNNs retain a large number of functional groups in glucose molecules, and glucose produces a certain degree of aromatization during hydrolysis, so a large number of CNNs remain in the water phase.[23] However, a large number of Fe₃O₄/CNNs remained at the oil−water interface, and only a small amount of Fe₃O₄/CNNs was distributed in the water phase, which reflected that after the CNNs were compounded with Fe₃O₄, they had better hydrophile−lipophile balance and were more easily distributed at the oil−water interface. The results show that Fe₃O₄/CNNs has good interfacial activity and migration ability, which can quickly reach the oil−water interface and promote oil−water separation.

3.6. Vibrating Sample Magnetometer (VSM) of Fe₃O₄/CNNs. The magnetic hysteresis loops for Fe₃O₄/CNNs is shown in Figure 7. From the figure, the saturation magnetization
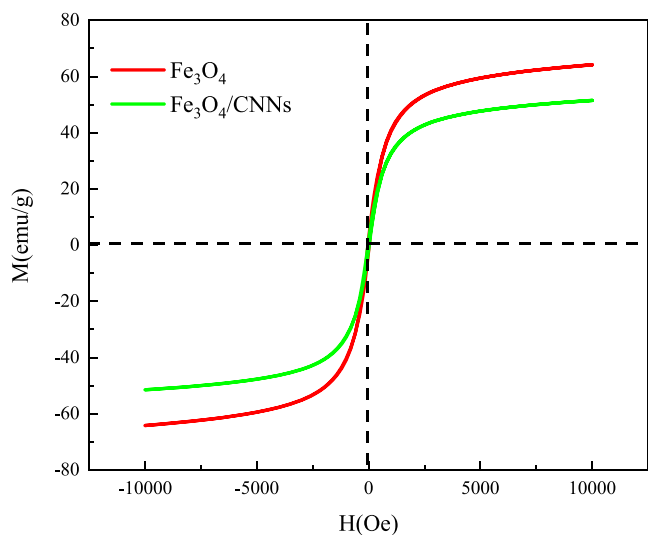
(Ms) of Fe₃O₄ is 64.14 emu/g, and the saturation magnetization of Fe₃O₄/CNNs is 51.46 emu/g. Compared with the saturation magnetization of Fe₃O₄, the saturation magnetization of the Fe₃O₄/CNNs has a significant decrease, which is mainly due to the CNNs shading the Fe₃O₄. At the same time, the hysteresis loop of the magnetic demulsifier passes through the origin, which proves that the magnetic demulsifier has no residual magnetization intensity and coercive force.

3.7. Demulsification Performance of Samples. *3.7.1. Effect of Temperature on Demulsification Performance.* Temperature is one of the most important factors affecting demulsification efficiency. Increasing the demulsification temperature can provide energy to the small droplets dispersed in the oil phase, which is conducive to droplet coalescence and sedimentation. When adding the demulsifier, appropriately increasing the temperature is also beneficial for the demulsifier to reach the oil−water interface more quickly. As can be seen from Figure 8, a total of five temperatures were set on the X-axis
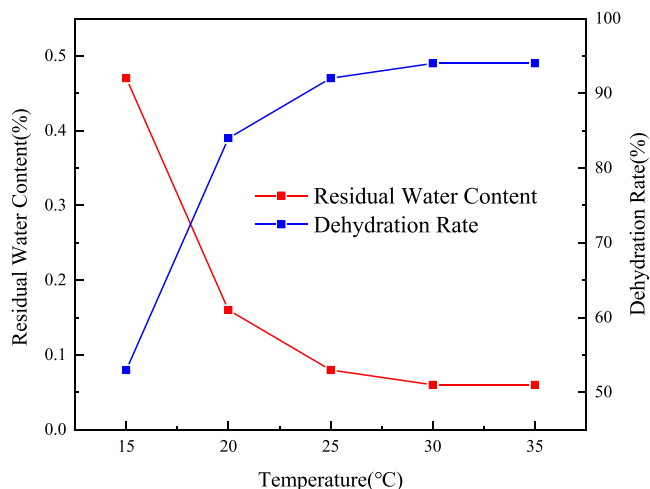
Figure 8. Dehydration rate of Fe₃O₄/CNNs at different temperatures.

(15, 20, 25, 30, and 35 °C). The dehydration rate gradually increased when the experimental temperature increased. In addition, the dehydration rate of Fe₃O₄/CNNs also reached the highest when the temperature reached 35 °C and the residual water content of Fe₃O₄/CNNs could be reduced to 0.08%. Meanwhile, Figure 8 also shows that the residual water content in the oil phase of Fe₃O₄/CNNs decreased by 0.02% when the temperature was increased from 25 to 35 °C. This shows that when the temperature reached 25 °C, even if continued to increase the temperature, the increase in the dehydration rate of the demulsifier is extremely limited, therefore, the demulsification temperature is set at 25 °C.


Figure 7. Magnetic hysteresis loops for synthesized products.

3.7.2. Effect of Time on Demulsification Performance. Time is also an important factor affecting the efficiency of demulsification. Too short a demulsification time is not conducive to the demulsifier completely acting on the oil–water interface to promote droplet coalescence and sedimentation, while too long a time is also not conducive to practical applications. Therefore, it is important to set the time reasonably. As can be seen in Figure 9, the *X*-axis was set for
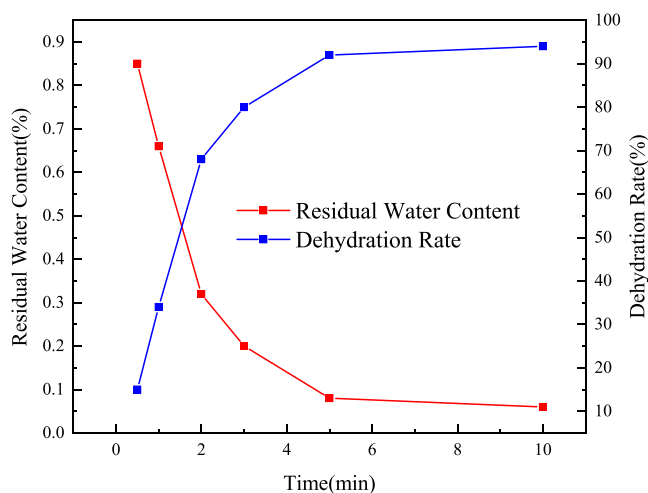
Figure 9. Dehydration rate of Fe_3O_4/CNNs at different times.

six times, respectively (0.5, 1, 2, 3, 5, and 10 min). The dehydration rates of the Fe_3O_4/CNNs were significantly increased with increasing time, and the residual water content of Fe_3O_4/CNNs could be reduced to 0.06% at 10 min. However, it is worth noting that there is only a slight decrease in the residual water content in the oil phase during the increase of the time from 5 to 10 min.

3.7.3. Effect of Demulsifier Dosage on Demulsification Performance. It can be seen from Figure 10 that the amount of residual water content in the oil phase is gradually reduced with the increase of the demulsifier dosage. The decreasing trend was very obvious when the demulsifier dosage increased from 200 to 600 ppm. The highest dehydration rate reached when the demulsifier dosage was 800 ppm, and when the demulsifier
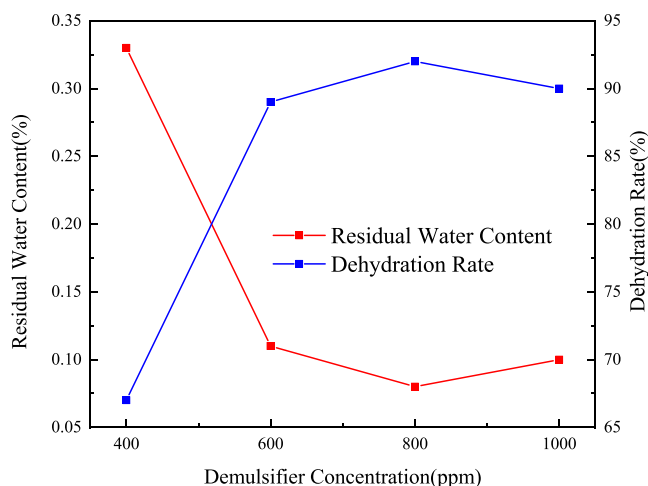
Figure 10. Dehydration rate of Fe_3O_4/CNNs for different demulsifier dosages.

dosage increased to 1000 ppm, the demulsification ability became weaker and even led to the increase of the residual water content in the oil phase. This is due to the fact that when the dosage of the demulsifier increases to a certain level, the demulsifier molecule at the oil–water interface has reached saturation, and continuing to increase the demulsifier will lead to emulsification instead.[24]

3.7.4. Recycling Performance Testing. Figure 11 shows the recycling performance of the Fe_3O_4/CNNs. When the Fe_3O_4/
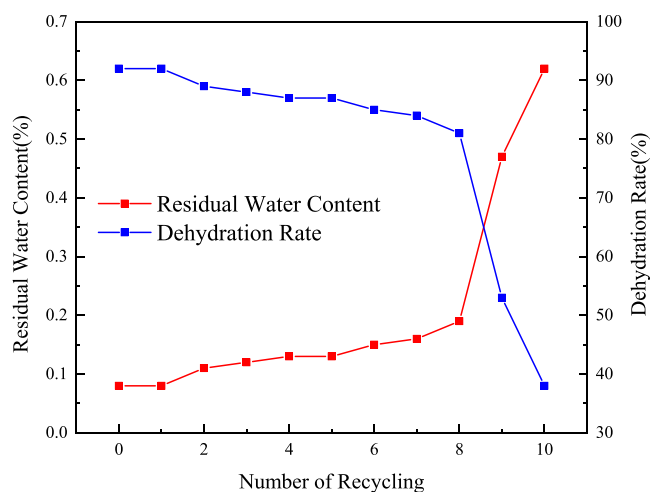
Figure 11. Recycling performance of Fe_3O_4/CNNs.

CNNs was recycled eight times, the residual water content in the oil phase did not change much and only increased by 0.11%. This shows that the Fe_3O_4/CNNs can be recycled without affecting their performance. Meanwhile, when the ninth demulsification experiment was conducted, the dehydration rate increased significantly. This indicates that a certain amount of oil phase was adsorbed on the surface of the Fe_3O_4/CNNs which could not be washed away completely, making the Fe_3O_4/CNNs adsorption sites less, so the demulsification performance was affected. Therefore, it can be concluded that the Fe_3O_4/CNNs prepared in this work performs well in the tests of recycling experiments and has good recyclability.

3.7.5. Comparison of Fe3O4/CNNs with Other Demulsifiers. Figure 12 shows the demulsification performance of Fe_3O_4/CNNs and four commercial demulsifiers under the same demulsification conditions (30 °C, 800 mg/L, 5 min). It can be clearly observed that the demulsification performance of Fe_3O_4/CNNs is significantly higher than that of the commercial demulsifier. The dehydration rate of the four commercial demulsifiers was not more than 40%. These fully demonstrate the advantages of rapid demulsification of Fe_3O_4/CNNs at 30 °C. Meanwhile, the economic feasibility of Fe_3O_4/CNNs is considerable. First of all, Fe_3O_4/CNNs can complete the separation of oil and water at 30 °C, which can save the cost of heating equipment such as heating furnace in practical application. Second, Fe_3O_4/CNNs have excellent demulsification performance, which can complete oil–water separation in a very short time, saving the operation cost of various equipment in the production process. Finally, the synthesis process of Fe_3O_4/CNNs is simple and the synthetic raw materials are easy to obtain. The synthetic cost of this demulsifier is lower than that of most other nanodemulsifiers or polymer demulsifiers. Therefore, Fe3O4/CNNs has certain economic feasibility.
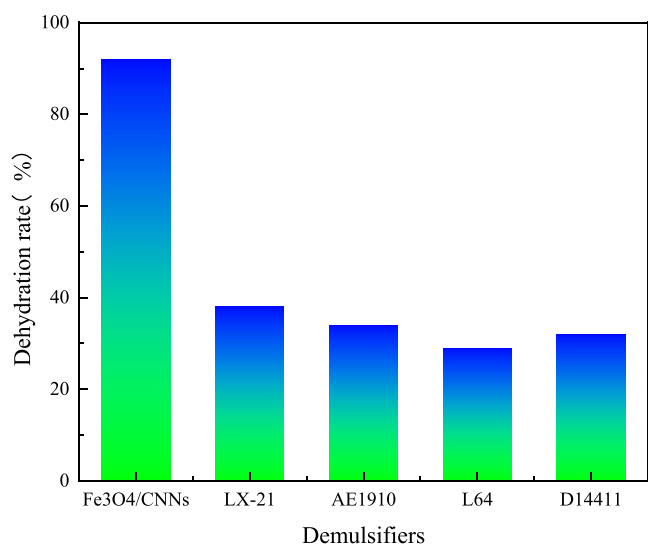
Figure 12. Demulsification rates of Fe_3O_4/CNNs and commercial demulsifiers.

Figure 14. Demulsification mechanism of Fe_3O_4/CNNs.

3.8. Demulsification Mechanism. Figure 13 shows a schematic diagram of the dehydration process of water-in-toluene emulsions. As can be seen in Figure 13d, the emulsion was dispersed with dense and fine droplets, and these droplets were stable and did not coalesce, because they are negatively charged and repulsive. Thus the emulsion remained relatively stable. In Figure 13b, the number of droplets became less and the diameter of droplets became larger. This indicates that when the magnetic demulsifier was added to the emulsion, the stability of the emulsion was broken, and the small droplets were coalesced rapidly and separated by the difference of density between oil and water. Therefore, the demulsification mechanism of Fe_3O_4/CNNs is rationalized.

Figure 14 shows the demulsification process of Fe_3O_4/CNNs. From the preparation process, due to the addition of oleic acid, Fe_3O_4/CNNs is lipophilic. At the same time, CNNs are hydrolyzed from glucose and are hydrophilic. When the Fe_3O_4/CNNs were added to the emulsion, they can quickly reach the oil−water interface, replacing the emulsifier molecules.

At this time, the lipophilic part of the magnetic emulsion breaker can "grab" the oil phase, breaking the relative stability of the oil-in-water emulsion, releasing small droplets of water in the emulsion. Fine water droplets were bound together through the hydrophilic part of the magnetic emulsion breaker, and the stability of the oil−water interface film was broken, and the oil−water phases were gradually separated due to different densities. Second, because CNNs contain a conjugated aromatic ring structure, this structure can attract oil droplets through $\pi-\pi$ bonding with the oil phase in the emulsion, then the Fe_3O_4/CNNs' demulsification ability is enhanced, and thus faster demulsification is achieved. Then, the Fe_3O_4/CNNs was adsorbed by the magnetic field, which further increased the chance of small oil droplets coalescing and becoming large oil droplets.[10] In addition, CNNs and Fe_3O_4 are both nanoscale materials with a large specific surface area, and there are more spots for adsorption on the material surface, so higher dehydration rates can be obtained.

4. CONCLUSIONS

In this paper, an effective method was reported to dehydrate from water-in-oil emulsion using Fe_3O_4/CNNs as a demulsifier. The composite material was synthesized in one step by a
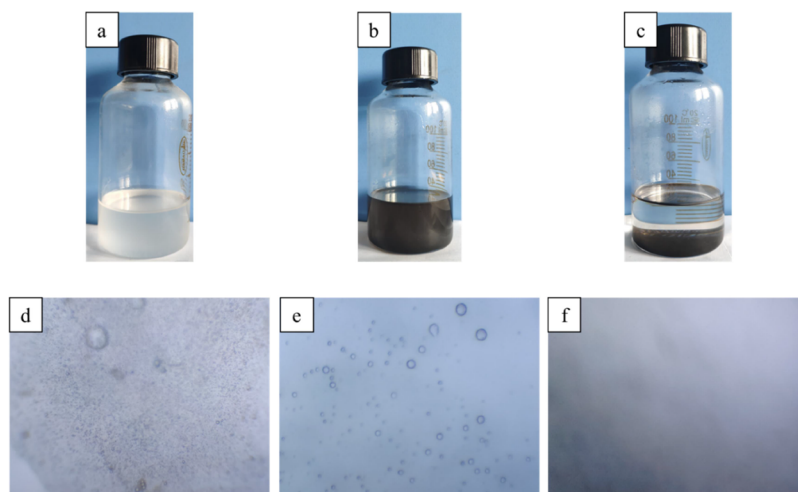
Figure 13. (a) Water-in-toluene emulsion; (b) Adding of Fe_3O_4 / CNNs to (a); (c) Separation of toluene and water; (d) Microscope image in (a); (e) Microscope image of the demulsification process with small droplets coalesced; (f) Microscope image of the oil phase after separation of the oil and water phases, with no obvious emulsified water present.

solvothermal method. The demulsification experiments showed that the Fe_3O_4/CNNs have good demulsification performance, and the best dehydration rate is 92% (800 ppm, 25 °C, 5 min). After 10 cycles of recycling experiments on the Fe_3O_4/CNNs, the dehydration rate of the first eight times could be maintained above 80%, indicating a good recovery ability. Speculation on the demulsification mechanism suggests that the Fe_3O_4/CNNs is amphiphilic and can quickly reach the oil−water interface and destroy the oil−water interface film. Compared with other magnetic demulsifiers, the preparation process of the Fe_3O_4/CNNs is simple and does not cause pollution to the environment, which has certain guiding significance for future research of magnetic demulsifiers.

■ AUTHOR INFORMATION

Corresponding Author

Lixin Wei − *Key Laboratory of Enhanced Oil Recovery, Northeast Petroleum University, Ministry of Education, Daqing 163318, China;* orcid.org/0000-0001-5596-8789; Email: weilixin73@163.com

Authors

Shijun Guo − *Key Laboratory of Enhanced Oil Recovery, Northeast Petroleum University, Ministry of Education, Daqing 163318, China; Heilongjiang Provincial Key Laboratory of Oilfield Applied Chemistry and Technology, Daqing Normal University, Daqing 163712, China*

Lin Zhang − *Key Laboratory of Enhanced Oil Recovery, Northeast Petroleum University, Ministry of Education, Daqing 163318, China;* orcid.org/0000-0002-9740-1980

Complete contact information is available at:
https://pubs.acs.org/10.1021/acsomega.2c07050

Notes

The authors declare no competing financial interest.

■ ACKNOWLEDGMENTS

■ REFERENCES

(1) Huang, Z.; Li, P.; Luo, X.; Jiang, X.; Liu, L.; Ye, F.; Kuang, J.; Luo, Y.; Mi, Y. Synthesis of a Novel Environmentally Friendly and Interfacially Active CNTs/SiO2 Demulsifier for W/O Crude Oil Emulsion Separation. *Energy Fuels* **2019**, *33*, 7166−7175.

(2) Nikkhah, M.; Tohidian, T.; Rahimpour, M. R.; Jahanmiri, A. Efficient demulsification of water-in-oil emulsion by a novel nano-titania modified chemical demulsifier. *Chem. Eng. Res. Des.* **2015**, *94*, 164−172.

(3) Ali, N.; Zhang, B.; Zhang, H.; Li, W.; Zaman, W.; Tian, L.; Zhang, Q. Novel Janus magnetic micro particle synthesis and its applications as a demulsifier for breaking heavy crude oil and water emulsion. *Fuel* **2015**, *141*, 258−267.

(4) Xu, H.; Jia, W.; Ren, S.; Wang, J. Novel and recyclable demulsifier of expanded perlite grafted by magnetic nanoparticles for oil separation from emulsified oil wastewaters. *Chem. Eng. J.* **2018**, *337*, 10−18.

(5) Wang, F.; Fang, S.; Duan, M.; Xiong, Y.; Wang, X. Synthesis of a novel demulsifier by one-pot synthesis using two PEO-PPO demulsifiers as materials and the study of its demulsification performance. *Sep. Sci. Technol.* **2019**, *54*, 1233−1240.

(6) Kuang, J.; Mi, Y.; Zhang, Z.; Ye, F.; Luo, Y. A hyperbranched poly(amido amine) demulsifier with trimethyl citrate as initial cores and its demulsification performance at ambient temperature. *J. Water. Process. Eng.* **2020**, *38*, No. 101542.

(7) Agah, M.; Binazadeh, M.; Baghulifard, N.; Sarani, M. Demulsification of saline-in-crude oil via biocompatible cellulose derivative polymers. *Fuel* **2022**, *311*, No. 122533.

(8) Abullah, M.; Al-Lohedan, H. A.; Attah, A. M. Synthesis and application of amphiphilic ionic liquid based on acrylate copolymers as demulsifier and oil spill dispersant. *J. Mol. Liq.* **2016**, *219*, 54−62.

(9) Aau, A.; Ims, A.; Ah, B.; Aas, A.; Aaa, A. Magnetic polyester bis-mpa dendron nanohybrid demulsifier can effectively break water-in-crude oil emulsions-sciencedirect. *J. Mater. Res. Technol.* **2020**, *9*, 13411−13424.

(10) Lü, T.; Shuang, Z.; Qi, D.; Dong, Z.; Zhao, H. Enhanced demulsification from aqueous media by using magnetic chitosan-based flocculant. *J. Colloid Interface Sci.* **2018**, *518*, 76.

(11) Zhao, H.; Zhang, C.; Qi, D.; Ting, L.; Zhang, D. One-step synthesis of polyethylenimine-coated magnetic nanoparticles and its demulsification performance in surfactant-stabilized oil-in-water emulsion. *J. Dispersion Sci. Technol.* **2019**, *40*, 231−238.

(12) Li, S.; Li, N.; Yang, S.; Liu, F.; Zhou, J. The synthesis of a novel magnetic demulsifier and its application for the demulsification of oil-charged industrial wastewaters. *J. Mater. Chem. A* **2014**, *2*, 94−99.

(13) Xie, P.; Yuan, W.; Liu, X.; Peng, Y.; Wu, Z. Advanced carbon nanomaterials for state-of-the-art flexible supercapacitors. *Energy Storage Mater.* **2020**, *36*, 56−76.

(14) Hu, C.; Qu, J.; Xiao, Y.; Zhao, S.; Chen, H.; Dai, L. Carbon nanomaterials for energy and biorelated catalysis: recent advances and looking forward. *ACS Cent. Sci.* **2019**, *5*, 389−408.

(15) Loh, K. P.; Ho, D.; Chiu, G. N. C.; Leong, D. T.; Pastorin, G.; Chow, K. H. Clinical applications of carbon nanomaterials in diagnostics and therapy. *Adv. Mater.* **2018**, *30*, No. 1802368.

(16) Huang, Z.; Luo, X.; Mi, Y.; Wu, G.; Wang, C.; Liu, L.; Ye, F.; Luo, Y. Magnetic recyclable carbon nanotubes and its demulsification performance in oily wastewater. *Sep. Sci. Technol.* **2021**, *56*, 2150−2158.

(17) Li, G.; Guo, C.; Sun, C.; Ju, Z.; Yang, L.; Xu, L.; Qian, Y. A facile approach for the synthesis of uniform hollow carbon nanospheres. *J. Phys. Chem. C* **2008**, *112*, 1896−1900.

(18) Zhang, P.; Qiao, Z.; Dai, S. Recent advances in carbon nanospheres: synthetic routes and applications[J]. *Chem. Commun.* **2015**, *51*, 9246−9256.

(19) Zhang, P.; Qiao, Z. A.; Dai, S. Recent advances in carbon nanospheres: synthetic routes and applications. *Chem. Commun.* **2015**, *51*, 9246−9256.

(20) Gupta, A.; Kour, R.; Brar, L. K. Facile synthesis of carbon nanospheres from saccharides for photocatalytic applications. *SN Appl. Sci.* **2019**, *1*, 1−10.

(21) Gao, J.; Ran, X.; Shi, C.; Cheng, H.; Cheng, T.; Su, Y. One-step solvothermal synthesis of highly water-soluble, negatively charged superparamagnetic Fe_3O_4 colloidal nanocrystal clusters. *Nanoscale* **2013**, *5*, 7026−7033.

(22) Wilson, D.; Langell, M. A. XPS analysis of oleylamine/oleic acid capped Fe_3O_4 nanoparticles as a function of temperature. *Appl. Surf. Sci.* **2014**, *303*, 6−13.

(23) Cai, H.; Lin, X.; Qin, Y.; Luo, X. Hydrothermal synthesis of carbon microsphere from glucose at low temperature and its adsorption property of uranium(vi). *J. Radioanal. Nucl. Chem.* **2017**, *311*, 695−706.

(24) Yu, H.; Gu, L.; Wu, S.; Dong, G.; Zhang, D. Hydrothermal carbon nanospheres assisted-fabrication of pvdf ultrafiltration membranes with improved hydrophilicity and antifouling performance. *Sep. Purif. Technol.* **2020**, *247*, No. 116889.